Materials Transactions, JIM, Vol. 36, No. 7 (1995), pp. 962 to 971

Hard Magnetic Properties of Nanocrystalline Fe-Rich Fe-Nd-B Alloys Prepared by Partial Crystallization of Amorphous Phase

A. Inoue*, A. Takeuchi*, A. Makino** and T. Masumoto*

*Institute for Materials Research, Tohoku University, Sendai 980-77, Japan
**Central Research Laboratory, Alps Electric Co., Ltd., Nagaoka 940, Japan

When Fe-rich Fe-Nd-B amorphous alloys containing 88 to 90 at% Fe are annealed for 60–300 s at 923–1023 K, the annealed alloys have the nanostructure consisting of bcc-Fe, $Fe_{14}Nd_2B$ and remaining amorphous phases and exhibit rather good hard magnetic properties. The best hard magnetic properties of remanence (B_r), coercive field ($_iH_c$) and maximum energy product ($(BH)_{max}$) are 1.14 T, 260 kA/m and 117 kJ/m^3, respectively, for $Fe_{90}Nd_7B_3$, 1.28 T, 252 kA/m and 146 kJ/m^3, respectively, for $Fe_{89}Nd_7B_4$ and 1.22 T, 240 kA/m and 130 kJ/m^3 for $Fe_{88}Nd_8B_4$. The mean particle sizes of these crystallites in the optimum annealing treatment are 20 to 40 nm and the thickness of the intergranular amorphous layer is 10 to 30 nm. The amorphous layer contains Nd concentrations much higher than the nominal concentration and the enrichment seems to be the reason for the residual existence of the amorphous phase at the high temperatures. The nanoscale $Fe_{14}Nd_2B$ particles are surrounded by the bcc-Fe and amorphous phases. The three constituent phases have ferromagnetism and their Curie temperatures for the $Fe_{89}Nd_7B_4$ alloy annealed for 300 s at 923 K are about 1040 K for bcc-Fe and 630 K for $Fe_{14}Nd_2B$. The further increase in annealing temperature and time causes the decrease in hard magnetic properties presumably because of the grain growth of bcc-Fe and $Fe_{14}Nd_2B$ phases resulting from the disappearance of the residual amorphous phase. The coexistence of bcc-Fe, $Fe_{14}Nd_2B$ and amorphous phases on a subnanoscale is important for the achievement of the rather good hard magnetic properties and hence the bcc-Fe and amorphous phases seem to act as an effective magnetic exchange-coupled medium. The simultaneous achievement of the high B_r and $(BH)_{max}$ values in the residual existence of the amorphous phase for the Fe-rich alloys containing about 90 at% Fe is believed to be the first evidence and has significant engineering importance because of the expectations of high deformability and high cost performance.

(Received January 30, 1995)

Keywords: *hard magnetic alloy, iron-rich alloy, iron-neodymium-boron alloy, rapid solidification, amorphous alloy, crystallization, nanoscale mixed structure, intergranular amorphous phase, high remanence*

I. Introduction

For the last four years, we have carried out systematic studies[1]-[7] on the formation of an amorphous phase in Fe-rich Fe-M-B (M=transition and lanthanide metals) alloys containing more than about 87 at% Fe, their crystallization behavior to nanoscale mixed phases and nanocrystallization-induced characteristics. As a result, we have succeeded in fabricating excellent soft magnetic alloys with a nanostructure consisting of nanoscale bcc grains and intergranular amorphous phase in Fe-Zr-B[1], Fe-Hf-B[2] and Fe-Nb-B[4] systems. It is to be noticed that their nanocrystalline alloys exhibit high permeability reaching 50000 combined with high saturation magnetization exceeding 1.5 T resulting from high Fe concentrations of 87 to 90 at%. It has subsequently been found[8] that the partial crystallization of an amorphous $Fe_{90}Nd_7B_3$ alloy into a nanoscale mixture of bcc-Fe, bct-$Fe_{14}Nd_2B$ and intergranular amorphous phases causes the appearance of rather good hard magnetic properties, *e.g.*, the remanence of 1.14 T, the coercive field of 260 kA/m and the maximum energy product of 117 kJ/m^3. This result indicates the possibility that much better hard magnetic properties can be obtained in the coexistence of an amorphous phase as well as in the Fe-rich alloy containing as much as about 90 at% Fe. Thus, one can expect that the formation of the nanoscale mixed structures caused by the residual existence of amorphous phase in the Fe-M-B systems is a useful structural control method for the achievement of good hard magnetic properties as well as good soft magnetic properties. It has recently been reported[9]-[12] that nanocrystalline alloys consisting mainly of Fe_3B and $Fe_{14}Nd_2B$ phases are obtained by crystallization of amorphous Fe-Nd-B alloys with low neodymium (about 6 at%) and high boron (about 18 at%) concentrations and exhibit a high remanence of about 1.2 T and maximum energy products $(BH)_{max}$ of 100 to 138 kJ/m^3. Similarly, nanocrystalline alloys consisting of $Fe_{14}Nd_2B$ and α-Fe at Fe-rich compositions of about 82 to 88 at% Fe exhibit high remanence of about 1.0 T and maximum energy products of about 70 to 150 kJ/m^3 [13]-[20]. The nanocrystalline mixture of the Fe-rich alloys has been obtained either by crystallization of an amorphous phase or by control of cooling rate from melt. Although the maximum energy products are considerably smaller than those[21] for the stoichiometric $Fe_{14}Nd_2B$ compound, the nanocrystalline magnets have some advantages[22][23] in that the high $(BH)_{max}$ values are maintained even in a fine powder form and the degradation of $(BH)_{max}$ with increasing temperature is sluggish. The former advantage is quite attractive for the application to bond magnets with good formability in a mixed state of resin.

As described above, the previous results indicate that the maximum hard magnetic properties are obtained in the nanocrystalline state without residual amorphous phase, i.e., $Fe_3B+Fe_{14}Nd_2B$ phases for the B-rich Fe-Nd-B alloys and $Fe_{14}Nd_2B+\alpha$-Fe for the Fe-rich Fe-Nd-B alloys. In a previous paper[8], we have proposed the importance of the remaining amorphous phase for the formation of the nanocrystalline structure which enables the achievement of maximum hard magnetic properties. With the aim of confirming further the effectiveness of the nanoscale crystallites in coexistent with the residual amorphous phase, we have examined the compositional dependence of the as-quenched structure, crystallized microstructure and hard magnetic properties in rapidly solidified Fe-Nd-B alloys containing high Fe contents above 88%. In the subsequent study, we have found that further optimization of alloy composition and nanocrystalline structure causes a significant increase in $(BH)_{max}$ to 146 kJ/m^3 even for a Fe-rich $Fe_{89}Nd_7B_4$ alloy. This paper is intended to present the crystallization behavior, crystallized microstructure and hard magnetic properties of amorphous $Fe_{93-x}Nd_7B_x$ ($x=3$, 4 and 5 at%) alloys prepared by rapid solidification and to investigate the role of the intergranular amorphous phase in the formation of the nanoscale bcc-Fe and bct-$Fe_{14}Nd_2B$ phases and in the appearance of high $(BH)_{max}$ for the Fe-rich Fe-Nd-B alloys.

II. Experimental Procedure

Fe-Nd-B alloy ingots with 88 to 90 at% Fe concentrations were prepared by arc melting a mixture of pure Fe and Nd metals and pure B crystal in a purified argon atmosphere. Ribbons 15 μm thick and approximately 1 mm broad were obtained in an argon atmosphere using a single roller melt spinning equipment with a copper wheel rotating with a velocity of about 42 m/s. The amorphization of the ribbons was examined by X-ray diffractometry and conventional transmission electron microscopy (TEM). The annealing treatment was made in an evacuated state down to 8×10^{-3} Pa in sealed quartz tubes at temperatures between 873 and 1023 K and for durations between 60 and 3600 s. The crystallization behavior was examined by differential scanning calorimetry (DSC), X-ray diffractometry, conventional and high-resolution TEM. The DSC was made at a heating rate of 0.67 K/s. Alloy compositions in each constituent phase were also determined by using a nanobeam energy dispersive X-ray (EDX) spectroscope which was set in a high-resolution type transmission electron microscope (FEM-2010F). The thin foils for TEM observation were made by polishing electrolytically at approximately 223 K in a solution consisting of ethyl alcohol and perchloric acid with a mixing ratio of 9:1. The magnetization curves and hysteresis loops were measured with a vibrating sample magnetometer in fields up to 1.8 T. The coercive field and energy product were presented without correction of demagnetization field. The temperature dependence of magnetization was also measured in the temperature range of room temperature to 1073 K at a heating rate of 0.17 K/s in an evacuated state of 1.33×10^{-3} Pa.

III. Results

1. As-quenched and annealed structures

Figure 1 shows the relation between the alloy compositions of the $Fe_{93-x}Nd_7B_x$ ($x=3$, 4 and 5 at%), $Fe_{92-x}Nd_8B_x$ ($x=2$ and 4 at%) and $Fe_{89}Nd_9B_2$ alloys and the composition range in which an amorphous phase is formed in Fe-rich Fe-Nd-B alloys containing more than 88 at% Fe by rapid solidification. The glass formation range was taken from Refs. (8) and (21). As shown in the figure, these amorphous alloys are located at the Fe-rich composition side in the glass-formation range. The selection of the Fe-rich amorphous alloys is due to the following two factors; (1) the crystallization-induced alloys are mainly composed of the bcc-Fe phase because of the expectation of a high saturation magnetization, and (2) very little is known about the relation between microstructure and hard magnetic properties in the Fe-rich composition range more than 88 at% Fe. It has previously been reported that these Fe-rich amorphous alloys are located in the minimum solute concentration region where the $Fe_{14}Nd_2B$ phase with large magnetic anisotropy, in addition to α-Fe phase as a main phase, exists in an equilibrium state. It is therefore expected that the formation of the nanoscale mixed structure consisting of bcc-Fe and $Fe_{14}Nd_2B$ phases causes the appearance of rather high hard magnetic properties combined with high remanence even at the Fe-rich concentrations. Figure 2 shows the X-ray diffraction patterns of the rapidly solidified $Fe_{93-x}Nd_7B_x$ ($x=3$, 4 and 5 at%) alloys. The patterns consist only of broad peaks and no appreciable extra peak is observed. The wave vector ($K_p=4\pi\sin\theta/\lambda$) at the maximum position of the main broad peak is about 30.5 nm^{-1} which is nearly the same as those for amorphous $Fe_{90}M_7B_3$ (M=Zr or Hf) alloys[2][3]. In order to confirm the absence of any crystalline phase, a bright-field electron micrograph and a selected-area electron diffraction

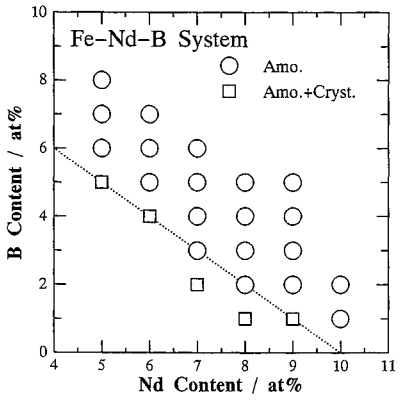

Fig. 1 Compositional range in which an amorphous phase is formed in rapidly solidified Fe-Nd-B alloys and alloy compositions of Fe-rich Fe-Nd-B alloys used in the present study.

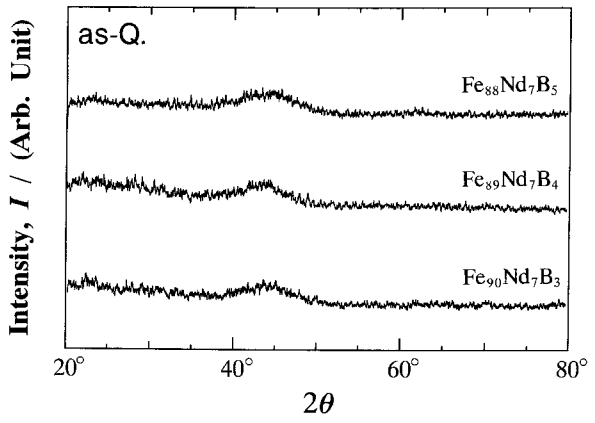

Fig. 2 X-ray diffraction patterns of rapidly solidified $Fe_{90}Nd_7B_3$, $Fe_{89}Nd_7B_4$ and $Fe_{88}Nd_7B_5$ alloys.

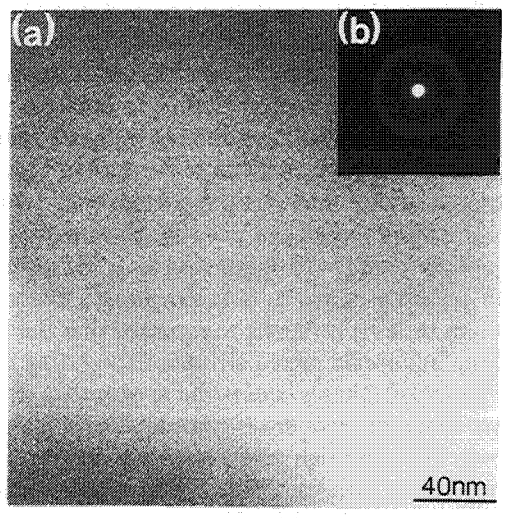

Fig. 3 Bright-field electron micrograph (a) and selected-area electron diffraction pattern (b) for a rapidly solidified $Fe_{89}Nd_7B_4$ alloy.

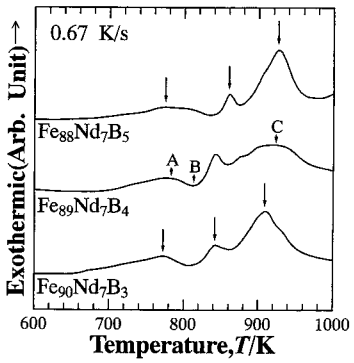

Fig. 4 DSC curves of $Fe_{90}Nd_7B_3$, $Fe_{89}Nd_7B_4$ and $Fe_{88}Nd_7B_5$ amorphous alloys.

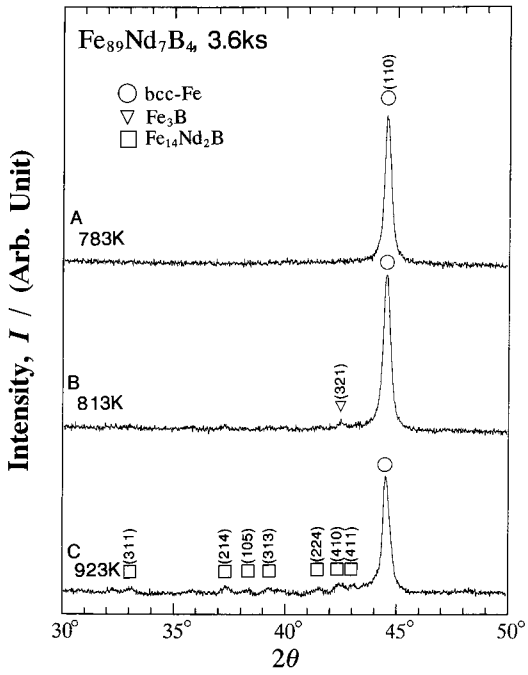

Fig. 5 X-ray diffraction patterns of an amorphous $Fe_{89}Nd_7B_4$ alloy annealed for 3.6 ks at the temperatures of A (783 K), B (813 K) and C (923 K).

pattern of the rapidly solidified $Fe_{89}Nd_7B_4$ alloy are shown in Fig. 3. The bright-field image shows only a modulated contrast typical for an amorphous phase and no contrast corresponding to the precipitation of a crystalline phase is seen over the whole image. The diffraction pattern also consists of halo rings. The results shown in Figs. 2 and 3 indicate clearly that the rapidly solidified phase in these Fe-rich alloys consists only of an amorphous phase.

Figure 4 shows the DSC curves of the amorphous $Fe_{93-x}Nd_7B_x$ (x=3, 4 and 5 at%) alloys. One can see three exothermic peaks marked with arrows, indicating that the crystallization of these amorphous alloys takes place through three stages. The peak temperatures of the three exothermic reactions are about 770, 840 and 910 K, respectively, for the $Fe_{90}Nd_7B_3$ alloy and tend to increase with increasing boron content. In order to examine the crystallization reaction corresponding to each exothermic peak, the X-ray diffraction patterns of the $Fe_{89}Nd_7B_4$ samples heated for 3.6 ks at 783, 813 and 923 K marked with A, B and C, respectively, are shown in Fig. 5. The diffraction peaks of these crystallites are identified to be a bcc-Fe phase at 783 K, bcc-Fe and bct Fe_3B phases at 813 K and bcc-Fe and $Fe_{14}Nd_2B$ phases at 923 K, indicating that the three exothermic peaks correspond to the precipitation of bcc-Fe, Fe_3B and $Fe_{14}Nd_2B$ phases, respectively. Figure 6 shows the bright- and dark-field images and the selected-area electron diffraction pattern of the rapidly solidified $Fe_{89}Nd_7B_4$ alloy subjected to heating for 300 s at 923 K corresponding to the temperature marked with C in Fig. 4. The dark-field images were taken from a part of the (110) bcc-Fe reflection ring. The electron diffraction patterns are identified to consist of amorphous and bcc-Fe phases and no reflection spots corresponding to $Fe_{14}Nd_2B$ are observed presumably because of a small volume fraction of the compound phase. Here, one can clearly see the residual existence of halo rings even for the sample heated for 300 s at 923 K. The

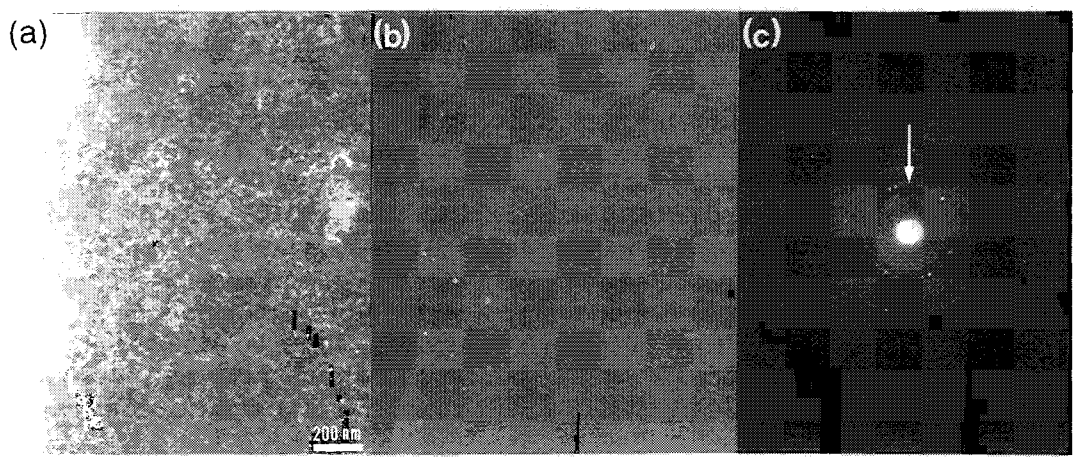

Fig. 6 Bright- and dark-field electron micrographs and selected-area electron diffraction pattern of an amorphous $Fe_{89}Nd_7B_4$ alloy annealed for 300 s at 923 K. The dark-field image (b) was taken from a part of (110) bcc-Fe reflection ring marked with an arrow in (c).

residual existence is consistent with the DSC data because the heating temperature corresponds to the temperature below the offset temperature of the third exothermic peak. Furthermore, one can notice that the diameter of the main halo ring in the electron diffraction patterns decreases for the annealed alloy, suggesting that the neodymium and boron contents in the remaining amorphous phase increase by the progress of the crystallization reaction leading to the increase in the precipitation amount of the bcc-Fe phase. The absence of the reflection spots of the Fe_3B phase in the electron diffraction pattern (Fig. 6(c)) and the disappearance of the Fe_3B diffraction peaks in Fig. 5 indicate that the Fe_3B phase is an intermediate phase, in agreement with the previous data[22][23] of the equilibrium phase diagram in Fe-Nd-B system. We have previously pointed out[8] that the Fe_3B phase is regarded as an incipient phase to cause the precipitation of the $Fe_{14}Nd_2B$ phase in the Fe-rich $Fe_{90}Nd_7B_3$ amorphous alloy.

2. Hard magnetic properties

Figure 7 shows the hysteresis *J-H* loops of the amorphous $Fe_{89}Nd_7B_4$ samples subjected to annealings at 923 K for different periods (t_a) of 180 to 3600 s. The remanence (B_r), coercive field ($_iH_c$) and maximum energy product $(BH)_{max}$ are measured to be 1.00 T, 196 kA/m and 108 kJ/m^3, respectively, for t_a=180 s, 1.28 T, 252 kA/m and 146 kJ/m^3, respectively, for t_a=300 s, 1.30 T, 241 kA/m and 118 kJ/m^3, respectively, for t_a=3600 s. It is to be noticed that the sample consisting of fine crystallites of bcc-Fe, $Fe_{14}Nd_2B$ and residual amorphous phase exhibits the large $(BH)_{max}$ value reaching 146 kJ/m^3 in spite of the Fe-rich composition. Similar high B_r and large $(BH)_{max}$ values are obtained for other Fe-rich $Fe_{90}Nd_7B_3$ and $Fe_{88}Nd_8B_4$ amorphous alloys subjected to optimum annealing treatment leading to the coexistent bcc-Fe, $Fe_{14}Nd_2B$ and residual amorphous phases, as exemplified for the hysteresis *J-H* loops in Fig. 8. The largest values of B_r, $_iH_c$ and $(BH)_{max}$ are 1.14 T, 260 kA/m and 117 kJ/m^3, respectively, for the $Fe_{90}Nd_7B_3$ alloy and

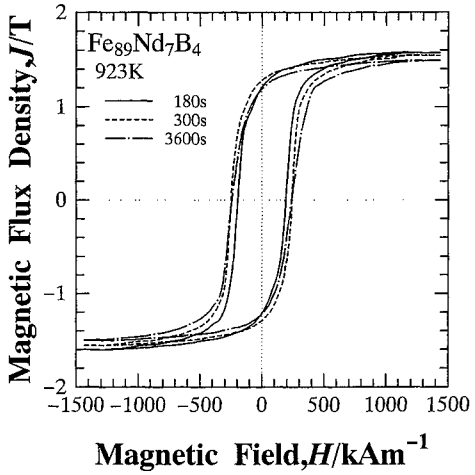

Fig. 7 Hysteresis *J-H* loops of an amorphous $Fe_{89}Nd_7B_4$ alloy annealed at 923 K for various periods of 180 to 3600 s.

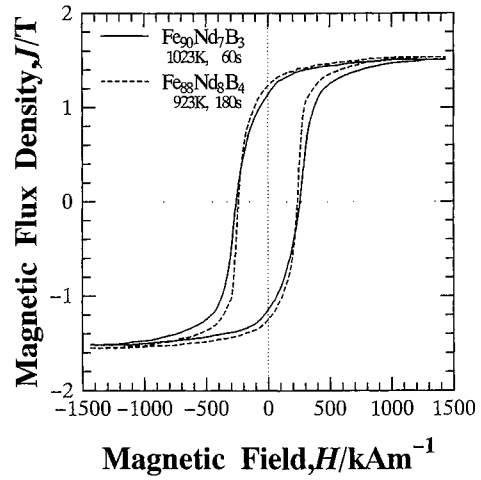

Fig. 8 Hysteresis *J-H* loops of amorphous $Fe_{90}Nd_7B_3$ and $Fe_{88}Nd_8B_4$ alloys subjected to optimum annealing for 60 s at 1023 K and for 300 s at 923 K, respectively.

1.22 T, 240 kA/m and 130 kJ/m^3, respectively, for the $Fe_{88}Nd_8B_4$ alloy. Figure 9 shows the changes in B_r, $_iH_c$ and $(BH)_{max}$ as a function of t_a at T_a=923 K corresponding to the temperature C in Fig. 4 for the amorphous $Fe_{89}Nd_7B_4$ and $Fe_{88}Nd_8B_4$ alloys. All the properties of B_r, $_iH_c$ and $(BH)_{max}$ show similar changes for both alloys. The maximum values of B_r, $_iH_c$ and $(BH)_{max}$ are obtained by annealing for 300 s and the deviation of t_a from 300 s causes the significant decrease in the hard magnetic properties. The appearance of the distinct maximum phenomenon in the changes in B_r, $_iH_c$ and $(BH)_{max}$ as a function of t_a indicates clearly that the largest $(BH)_{max}$ value for the present Fe-rich alloys is obtained in the optimal crystallization state where the structure consists of bcc-Fe, bct $Fe_{14}Nd_2B$ and residual amorphous phases. In comparison with the previous data on the hard magnetic properties and microstructure of Fe–Nd–B base alloys where the hard magnetic properties are induced on the basis of the magnetic exchange-coupling mechanism, the present hard magnetic alloys may be concluded to have the following features; (1) the appearance of the rather high $(BH)_{max}$ reaching 146 kJ/m^3 in the Fe-rich Fe–Nd–B alloy with low neodymium and boron concentrations, and (2) the largest $(BH)_{max}$ value is obtained in the mixed structure consisting of bcc-Fe, $Fe_{14}Nd_2B$ and remaining amorphous phases.

3. High resolution microstructure of partially crystallized Fe–Nd–B alloys

The information that the mixed structure including the residual amorphous phase in the Fe-rich alloys causes the rather high $(BH)_{max}$ value of 146 kJ/m^3 is very important for the interpretation of the mechanism for the appearance of the hard magnetism. With the aim of confirming the residual existence of the amorphous phase and clarifying the details of the nanoscale mixed structure, the partially crystallized structure of the amorphous $Fe_{89}Nd_7B_4$ alloy subjected to annealing for 300 s at 923 K was examined by high resolution TEM. Figure 10 shows the high-resolution TEM image (a) and nanobeam electron diffraction patterns (b) and (c) taken from the circular areas with the diameter of 1 nm in regions A and B, respectively. The distinct periodic fringe contrast with a small spacing of 0.20 nm corresponding to (111) of the bcc-Fe phase is seen in the region A and the nanobeam diffraction pattern (b) is also identified to be (111) of the bcc-Fe phase. On the other hand, the featureless modulated contrast typical for an amorphous phase is seen in the region B and the nanobeam diffraction pattern also consists of diffuse halo rings. These results indicate clearly that the region A with a particle size of about 12 nm corresponds to a bcc-Fe phase and the region B is composed of an amorphous phase. Furthermore, one can see the grain C where the periodic fringe contrast with a larger spacing of about 0.24 nm corresponding to (214) of the bct $Fe_{14}Nd_2B$ phase appears. It is thus concluded that the optimally annealed $Fe_{89}Nd_7B_4$ alloy exhibiting the highest $(BH)_{max}$ value has a mixed structure consisting of bcc-Fe, bct-$Fe_{14}Nd_2B$ and remaining amorphous phases. Figure 11 shows the EDX profiles (a) and (b) taken from

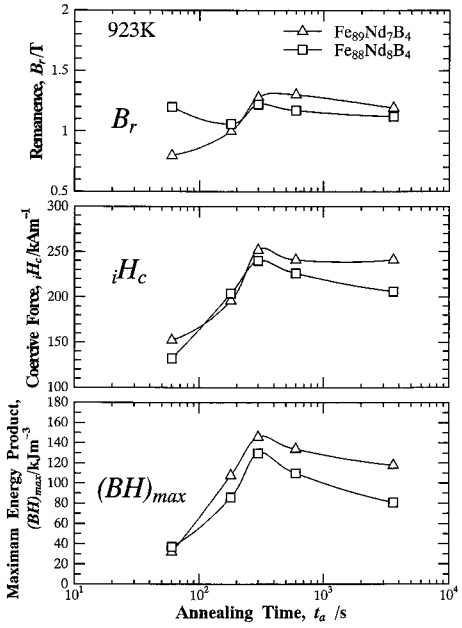

Fig. 9 Changes in the remanence (B_r), coercive field ($_iH_c$) and maximum energy product $(BH)_{max}$ as a function of annealing time (t_a) for amorphous $Fe_{89}Nd_7B_4$ and $Fe_{88}Nd_8B_4$ alloys annealed at 923 K.

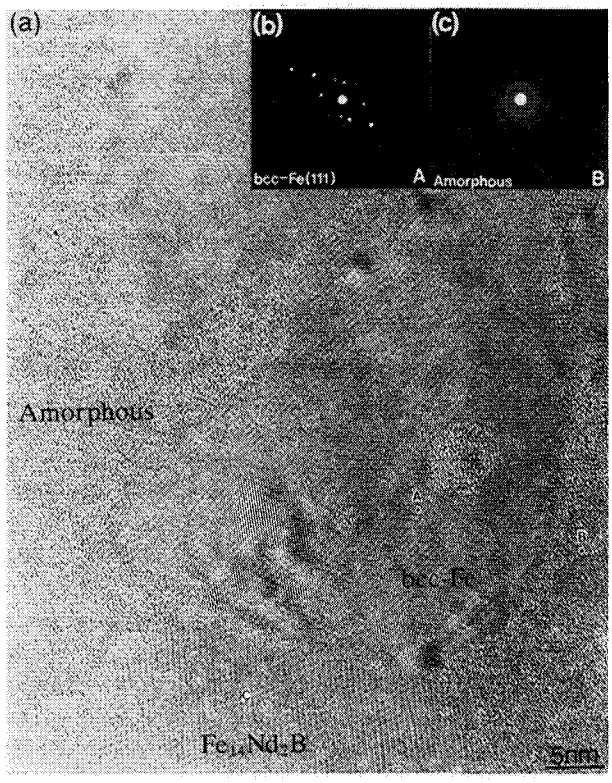

Fig. 10 High-resolution TEM image (a) and nanobeam electron diffraction patterns (b) and (c) taken from the regions with a diameter of 1 nm marked with A and B for an amorphous $Fe_{89}Nd_7B_4$ alloy annealed for 300 s at 923 K. The diffraction pattern (b) and (c) are identified to be (111) of the bcc-Fe phase and amorphous phase, respectively.

the regions A and B, respectively, in Fig. 10(a), along with the analytical iron and neodymium concentrations. The neodymium concentration is analyzed to be 0.5 at% for the bcc-Fe phase and 13.6 at% for the remaining amorphous phase and hence the neodymium element is concluded to be significantly enriched to the remaining amorphous phase. The increase in the thermal stability by the enrichment of neodymium seems to be the reason for the residual existence of the amorphous phase even after annealing for 300 s at 923 K. As exemplified for the high-resolution TEM image with a lower magnification in Fig. 12, the dispersion of the three constituent phases is rather homogeneous and their volume fractions appear to be nearly equal with each other. That is, the $Fe_{14}Nd_2B$ phase is surrounded by the bcc-Fe and remaining amorphous phase. The similar evidence on the formation of the nanoscale mixed structure consisting of the bcc-Fe, $Fe_{14}Nd_2B$ and remaining amorphous phases for the annealed samples with the highest $(BH)_{max}$ values is confirmed for the $Fe_{90}Nd_7B_3$ and $Fe_{88}Nd_8B_4$ alloys, as exemplified for the $Fe_{90}Nd_7B_3$ alloy annealed for 180 s at 923 K in Fig. 13. It is therefore presumed that the rather high $(BH)_{max}$ is due to the achievement of the exchange magnetic coupled state between $Fe_{14}Nd_2B$ particles with a particle size of about 30 nm through the bcc-Fe and amorphous phases with a spacing of about 10 nm. Furthermore, the high remanence reaching 1.3 T also seems to originate from the exchange magnetic coupled state between nanoscale bcc-Fe particles with high saturation magnetization via the remaining amorphous phase with ferromagnetism at room temperature.

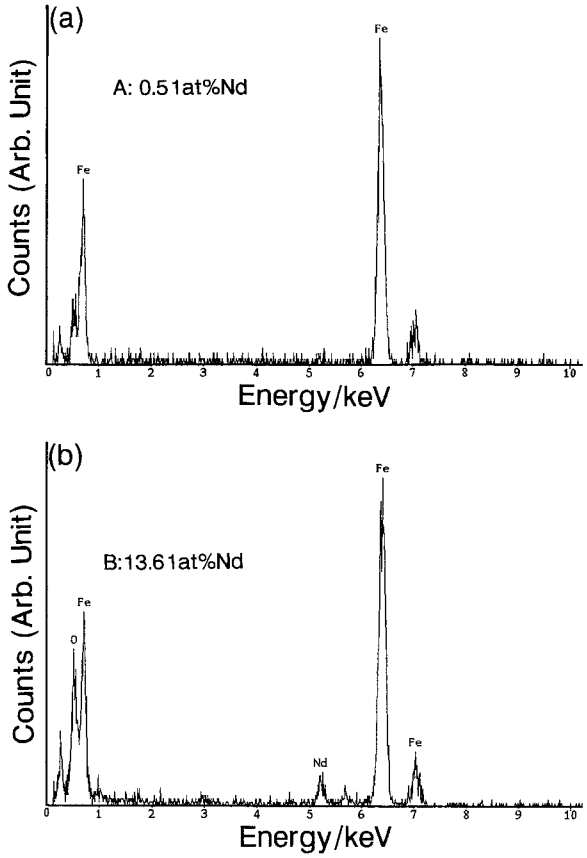

Fig. 11 Energy dispersive X-ray spectroscopy (EDX) profiles (a) and (b) taken from the regions A and B, respectively, in Fig. 10(a) for an amorphous $Fe_{89}Nd_7B_4$ alloy annealed for 300 s at 923 K.

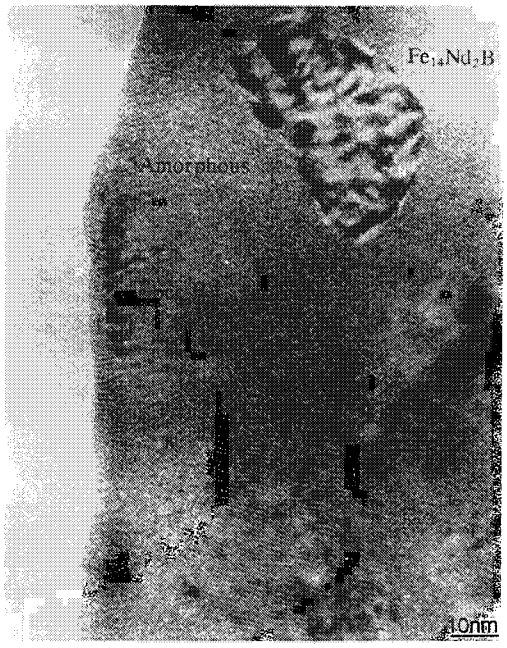

Fig. 12 High-resolution TEM image of an amorphous $Fe_{89}Nd_7B_4$ alloy annealed for 300 s at 923 K.

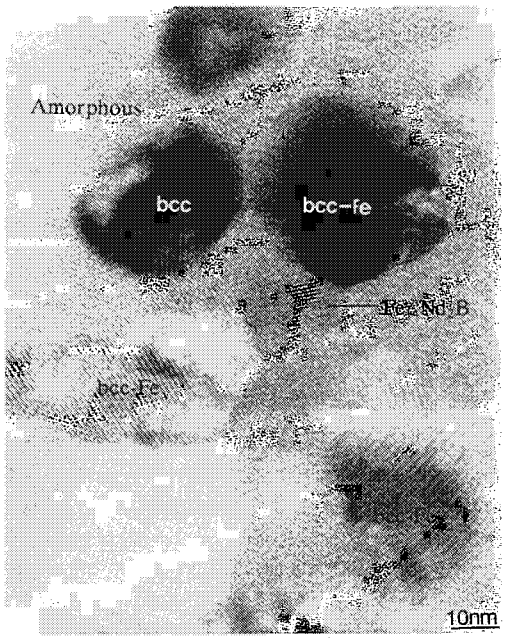

Fig. 13 High-resolution TEM image of an amorphous $Fe_{90}Nd_7B_3$ alloy annealed for 180 s at 923 K.

With the aim of further confirming the coexistence of the bcc-Fe, $Fe_{14}Nd_2B$ and remaining amorphous phases, the temperature dependence of magnetization (σ_s) of the amorphous $Fe_{89}Nd_7B_4$ alloy annealed for 300 s at 923 K was examined at a heating rate of 0.17 K/s in the temperature range of room temperature to 1073 K. As shown in

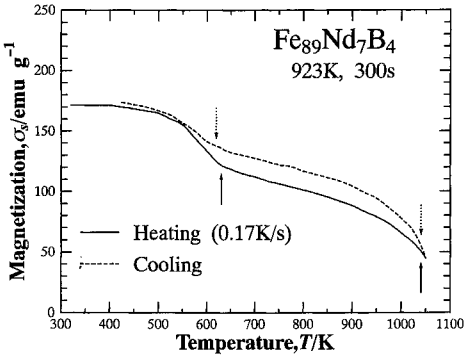

Fig. 14 Temperature dependence of magnetization (σ_s) of an amorphous $Fe_{89}Nd_7B_4$ alloy subjected to annealing for 300 s at 923 K.

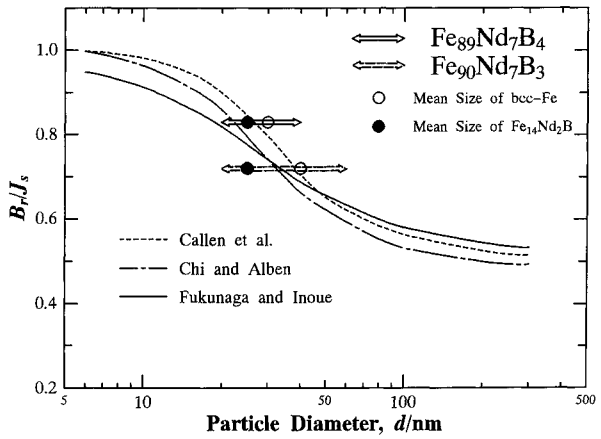

Fig. 15 Relation between the ratio of remanence to saturation magnetization (B_r/J_s) and mean particle diameters (d) of the bcc-Fe and $Fe_{14}Nd_2B$ phases for nanocrystalline $Fe_{90}Nd_7B_3$ and $Fe_{89}Nd_7B_4$ alloys. The theoretical curves taken from Refs. (26)–(28) are also shown for comparison.

Fig. 14, distinct two deflection points at about 630 and 1040 K are seen on the heating and cooling curves, as marked with arrows. Based on the previous results that the Curie temperature is 583 K for $Fe_{14}Nd_2B$[21] and 1043 K for α-Fe[24], the first deflection point at about 630 K and the second point at 1040 K are concluded to correspond to the Curie temperatures of the $Fe_{14}Nd_2B$ and α-Fe phases, respectively. Furthermore, from the compositional dependence of the Curie temperature of the amorphous Fe–Nd–B alloys[25], the Curie temperature of the remaining amorphous phase containing about 14 at% Nd is evaluated to be in the range of 400 to 460 K and almost independent of boron concentration. However, no appreciable deflection point on the σ_s(T) curve is seen in the temperature range, presumably because of the low volume fraction and low magnetization of the remaining amorphous phase.

IV. Discussion

1. Reason for the achievement of high remanence

The rather high maximum energy products of the present Fe-rich alloys are presumably due to the high remanences exceeding 1.2 T. Consequently, we discuss the reason for the achievement of the high remanence for the present nanophase alloys. The relation between the ratio of remanence to saturation magnetization (J_s), B_r/J_s and mean particle diameters of the constituent phases has theoretically been investigated[25]-[27] and the refinement of particle diameter has been reported to be essential for the achievement of high ratios of B_r to J_s. As shown for the J-H curves shown in Figs. 7 and 8, J_s is measured to be about 1.50 T for the $Fe_{90}Nd_7B_3$ alloy and 1.54 T for the $Fe_{89}Nd_7B_4$ alloy. The resulting B_r/J_s value is evaluated to be 0.72 for the 90%Fe alloy and 0.83 for the 89%Fe alloy. Furthermore, from the TEM images shown in Figs. 10, 12 and 13, the mean particle diameter of the bcc-Fe and $Fe_{14}Nd_2B$ phases is measured to be about 40 nm for the $Fe_{90}Nd_7B_3$ alloy and 30 nm for the $Fe_{89}Nd_7B_4$ alloy. No appreciable difference in the particle diameter between both alloys is seen for the $Fe_{14}Nd_2B$ phase and the difference results mainly from the bcc-Fe particles.

Figure 15 shows the plot of B_r/J_s as a function of mean particle diameter (d), along with the theoretical curves taken from Refs. (25) to (27). It is seen that the present data are in good agreement with the theoretically expected values. The agreement allows us to conclude that the high remanence originates from the interaction of nanoscale ferromagnetic particles with high saturation magnetization, i.e., from the magnetic coupling among the nanoscale bcc-Fe particles. The agreement also indicates that the refinement of the constituent phases is essential for the achievement of the high B_r values. It is therefore said that the residual existence of the amorphous phase leading to the formation of the nanophase mixture plays an important role in the appearance of the hard magnetic properties with the rather high energy products.

2. Relation between high $(BH)_{max}$ and the nanophase mixture

In comparison of the present alloy compositions of $Fe_{93-x}Nd_7B_x$ (x=3, 4 and 5 at%) with the pseudo-binary Fe-$Fe_{14}Nd_2B$ phase diagram of the Fe–Nd–B ternary system[21][22], one can see that the main constituent phase in the present alloys is the bct $Fe_{14}Nd_2B$ phase and the second phase is α-Fe. However, the volume fraction of the $Fe_{14}Nd_2B$ phase which is evaluated from the high-resolution TEM images is as small as about 10%. Furthermore, it is seen that the Fe–Nd–B alloy annealed at the optimum condition also contains the intergranular amorphous phase and the volume fraction of the remaining amorphous phase is approximately 15%. Besides, the neodymium concentration in the amorphous phase is about twice higher than the nominal neodymium concentration. It is therefore said that the volume fraction of the $Fe_{14}Nd_2B$ phase is considerably smaller than the value estimated from the equilibrium phase diagram. This tendency is consistent with the experimental result[8] that the volume fraction of the $Fe_{14}Nd_2B$ phase in the $Fe_{90}Nd_7B_3$

alloy is determined to be about 10% by high-resolution TEM. The small volume fraction of the $Fe_{14}Nd_2B$ phase with large magnetic anisotropy may be the reason for the rather small coercive field of 140 to 260 kA/m for the present Fe-rich Fe–Nd–B alloys. On the other hand, the small volume fraction of the $Fe_{14}Nd_2B$ phase also implies that a major part of the partially crystallized alloys is occupied by the bcc-Fe phase. The neodymium concentrations in the bcc-Fe particles are analyzed to be about 0.5 at% by the nanobeam EDX spectroscopy. Although the neodymium concentration is considerably lower than the nominal neodymium composition, it is much higher than the neodymium concentration which can be dissolved into α-Fe in an equilibrium state. The dissolution of neodymium in the bcc-Fe phase also seems to be the reason why the volume fraction of the $Fe_{14}Nd_2B$ phase is much smaller than that expected from the equilibrium phase diagram. The rather low neodymium concentration in the bcc-Fe phase allows us to expect that the bcc-Fe phase has a high remanence through the high saturation magnetization. Consequently, the high remanence of 1.28 T and the high saturation magnetization of 1.54 T are concluded to be due to the large amount of precipitation of the nanoscale bcc-Fe particles with low noedymium concentrations. It is shown in Figs. 10, 12 and 13 that the bcc-Fe particles with particle sizes of 20 to 40 nm disperse homogeneously at an interparticle spacing of about 10 nm and the intergranular phase field is mainly occupied by the remaining amorphous phase. It has previously been reported[29] that the residual amorphous phase with ferromagnetism can act as an effective coupling medium between bcc-Fe particles in the case where the spacing is smaller than the width ($\equiv$20 to 30 nm)[30] of the magnetic domain walls, leading to the achievement of high saturation magnetization. Similarly, the nanoscale $Fe_{14}Nd_2B$ particles with large magnetic anisotropy are also surrounded by the ferromagnetic bcc-Fe and amorphous phases. It has been pointed out[9] that the ferromagnetic bcc-Fe and amorphous phases can act as an effective magnetic exchange-coupled medium between nanoscale $Fe_{14}Nd_2B$ particles. The achievement of the magnetic exchange-coupled state is also supported from the result that the shape of the hysteresis *J-H* loop is smooth and neither any deflection point nor any step to multiple stages is seen in spite of the mixed nanophases. Consequently, it may be said that the present hard magnetic properties with high remanence generate by the simultaneous achievement of the following two magnetic couplings. That is, the high remanence is due to the magnetic coupling between nanoscale bcc-Fe particles via the intergranular ferromagnetic amorphous phase while the coercive field originates from the exchange magnetic coupling between nanoscale $Fe_{14}Nd_2B$ particles via ferromagnetic bcc-Fe and amorphous phases. The disappearance of the remaining amorphous phase caused by the increase in annealing temperature and time results in the drastic grain growth of the bcc-Fe and $Fe_{14}Nd_2B$ phases. As a result, the degree of the two magnetic coupling states decreases, leading to the simultaneous decrease in remanence and coercive field.

3. Dominant factors for the formation of the nanophase mixture

As described above, the key factor for the formation of the crystallization-induced nanostructure which enables the magnetic exchange coupling leading to the appearance of the high remanence and rather large energy product is the residual existence of the amorphous phase as the intergranular phase. Here, we investigate the reason why the remaining amorphous phase has high thermal stability and causes the formation of the nanoscale mixed structure. It is confirmed in Fig. 11 that the neodymium element is significantly enriched in the intergranular amorphous phase. It is also known that the crystallization temperature of the Fe–Nd–B amorphous alloys increases significantly with increasing neodymium and boron contents[23]. The analytical neodymium concentration in the remaining amorphous phase is about 14 at%. It is therefore estimated that the crystallization temperature increases from 850 K for the $Fe_{89}Nd_7B_4$ alloy to 940 K for the remaining amorphous $Fe_{71}Nd_{14}B_{15}$ alloy, from the previous data on the compositional dependence of crystallization temperature[25] for Fe–Nd–B amorphous alloys. In the present study, we do not have any data of boron concentration in the remaining amorphous phase, though boron should be significantly enriched into the amorphous phase. Therefore, it is reasonable to consider that the remaining amorphous phase has a crystallization temperature much higher than 860 K[25] for the $Fe_{82}Nd_{14}B_4$ alloy. The crystallization temperature estimated thus is consistent with the present result that the amorphous phase is maintained even after annealing for 300 s at 923 K. In addition, atom probe field ion microscopic (AP-FIM) results on the solute concentration profiles have recently been presented in the nanocrystallized structure consisting of fcc-Al and remaining amorphous phase in rapidly solidified Al–Ni–Ce amorphous alloys[31] and bcc-Fe and remaining amorphous phases in rapidly solidified Fe–Zr–B amorphous alloys[32]. The cerium element in the Al-based system and the zirconium and boron elements in the Fe–Zr–B system do not distribute homogeneously in the intergranular amorphous phase and are enriched more significantly in the vicinity of the intrerface between the amorphous and fcc-Al or bcc-Fe phases, as illustrated in Fig. 16. Besides, the solute element which is effective for the appearance of the steep concentration gradience has been reported[33] to satisfy with the following four criteria; (1) high melting temperature, (2) larger atomic size or large atomic size ratio among the constituent elements, (3) large negative heat of mixing against the major element, and (4) nearly zero solubility limit against the major element. These criteria are satisfied for neodymium and boron elements in Fe–Nd–B system. Consequently, the steep gradient distribution of the neodymium and boron elements is also expected to occur in the present intergranular amorphous phase for the Fe–Nd–B alloy, as illustrated in Fig. 16. As a result, the thermal stability of the remaining amor-

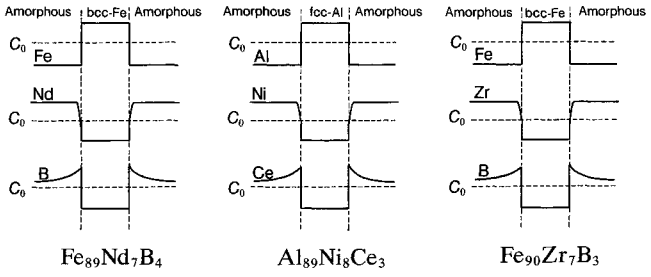

Fig. 16 Schematic illustration of the concentration profiles of Nd and B elements across the interface between bcc-Fe and remaining amorphous phase in an amorphous $Fe_{89}Nd_7B_4$ alloy subjected to the optimal annealing treatment for 300 s at 923 K. The previous data of partially crystallized $Al_{89}Ni_8Ce_3$ and $Fe_{90}Zr_7B_3$ alloys taken from Refs. (20) and (21) are also shown schematically for reference.

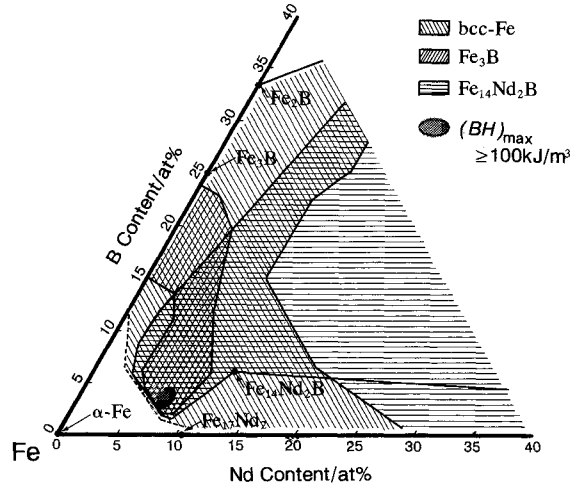

Fig. 17 Relation between the equilibrium phase diagram at room temperature for Fe-Nd-B ternary system and the composition range where the $(BH)_{max}$ values exceeding 100 kJ/m³ are obtained for the Fe-rich alloys containing more than 88 at% Fe. The equilibrium phase diagram was taken from Ref. (23).

phous phase is expected to increase through the combination of the following four effects[33]; (1) high gradient effect leading to the increase in thermal stability of an amorphous phase, (2) suppression of grain growth leading to the homogeneous dispersion of nanocrystalline particles, (3) suppression of heterogeneous nucleation at the interface between crystalline particle and amorphous matrix, and (4) gradual redistribution of alloy components among the constituent phases. It is therefore concluded that the present rather good hard magnetic properties combined with high remanence originate from the unique partial crystallization leading to the nanoscale mixed phases with particle sizes and alloy components which are appropriate for the appearance of hard magnetism through the remaining amorphous phase even at the Fe-rich compositions.

4. The role of Fe_3B in the formation of the nanophase mixture

It is shown in Section IV-2 that the residual existence of the amorphous phase with high thermal stability is the most dominant reason for the formation of the nanoscale mixed structure. In addition to the remaining amorphous phase, the Fe_3B phase seems to be also important for the formation of the nanophase structure through the modification of nucleation sites of the $Fe_{14}Nd_2B$ phase. Consequently, we investigate the contribution of the Fe_3B phase to the formation of the nanoscale mixed structure consisting of bcc-Fe, $Fe_{14}Nd_2B$ and residual amorphous phases in the Fe-rich $Fe_{90}Nd_7B_3$ and $Fe_{89}Nd_7B_4$ alloys. The existence of the three exothermic peaks corresponding to the bcc-Fe, Fe_3B and $Fe_{14}Nd_2B$ phases is shown in Fig. 4. Also, the confirmation that the second exothermic peak is due to the precipitation of the Fe_3B phase is obtained from the X-ray diffraction pattern shown in Fig. 5. Figure 17 shows the relation between the present alloy compositions and the equilibrium phase fields[23] at room temperature in Fe-Nd-B system. The nanophase alloys exhibiting energy products exceeding 100 kJ/m³ in the Fe-rich composition range above 88 at% Fe are limited to the composition range of 7 to 9%Nd and 3 to 4%B marked with a solid circle in Fig. 17 and the deviation of alloy composition from the composition range causes the decrease in $(BH)_{max}$ to down to 100 kJ/m³. Here, one can notice that the Fe-rich nanophase alloys with $(BH)_{max}$ above 100 kJ/m³ are located in the equilibrium phase field of α-Fe, Fe_3B and $Fe_{14}Nd_2B$ and the transition to the phase field of α-Fe and $Fe_{14}Nd_2B$ results in the decrease in $(BH)_{max}$. Although the reason for the existence of the Fe_3B phase in the high iron and low boron concentration range remains unclear, the coexistence of the Fe_3B phase seems to play a dominant role in the achievement of high $(BH)_{max}$ exceeding 100 kJ/m³. The results obtained by TEM and X-ray diffractometry indicate the disappearance of the Fe_3B phase in the sample heated up to the third exothermic peak marked with C in Fig. 4 and no evidence of the residual existence of the Fe_3B phase is obtained. These results allow us to presume that the Fe_3B phase appears as an intermediate phase in the transition stage from bcc-Fe+Am to bcc-Fe+$Fe_{14}Nd_2B$. The coexistence of the multiple phases of bcc-Fe+Fe_3B+$Fe_{14}Nd_2B$+Am including the Fe_3B phase seems to be important for the formation of the nanoscale mixed structure which is favorable for the achievement of high $(BH)_{max}$ values exceeding 100 kJ/m³ for the Fe-rich alloys. The effectiveness of the Fe_3B phase on the formation of the nanophase mixture is presumably because the Fe_3B phase causes the increase on the number of nucleation sites of the $Fe_{14}Nd_2B$ phase, in addition to the suppression of the growth of the bcc-Fe phase. It is reasonable to infer that the precipitation of the $Fe_{14}Nd_2B$ phase is easier at the high boron concentration site where the Fe_3B phase is in preexistence. Consequently, the useful contribution of the Fe_3B phase to the refinement of the mixed structure is thought to give rise to the result that the high $(BH)_{max}$ values exceeding 100 kJ/m³ for the Fe-rich alloys are obtained only in the mixed phase field of α-Fe+$Fe_{14}Nd_2B$ containing a small amount of Fe_3B.

V. Summary

The relation between the crystallization-induced microstructure and hard magnetic properties has been examined for amorphous Fe–Nd–B alloys containing more than 88 at% Fe prepared by rapid solidification, with the aim of fabricating a hard magnetic material with a Fe-rich composition. The results obtained are summarized as follows:

(1) Fe-rich Fe–Nd–B alloys with Fe concentrations between 88 and 90 at% were amorphized by rapid solidification. These amorphous alloys crystallized through three stages of Am→Am′+bcc-Fe→Am″+bcc-Fe+bct-Fe_3B → Am‴ + bcc-Fe + bct-$Fe_{14}Nd_2B$(+Fe_3B)→α-Fe+$Fe_{14}Nd_2B$. The bcc-Fe, Fe_3B and $Fe_{14}Nd_2B$ phases precipitate in each temperature range of 710 to 800, 810 to 850 and 860 to 960 K, respectively.

(2) The highest hard magnetic properties were obtained by annealing for 180 s at 923 K for $Fe_{90}Nd_7B_3$ and for 300 s at 923 K for $Fe_{89}Nd_7B_4$ and $Fe_{88}Nd_8B_4$ and the deviation from the annealing condition causes the degradation of the hard magnetic properties. The highest values of remanence, coercive field and maximum energy product are 1.14 T, 260 kA/m, 117 kJ/m^3, respectively, for the $Fe_{90}Nd_7B_3$ alloy, 1.28 T, 252 kA/m and 146 kJ/m^3, respectively, for the $Fe_{89}Nd_7B_4$ alloy and 1.22 T, 240 kA/m and 130 kJ/m^3, respectively, for the $Fe_{88}Nd_8B_4$ alloy.

(3) The Fe–Nd–B alloys with the largest energy products have a nanostructure consisting of bcc-Fe, $Fe_{14}Nd_2B$ and remaining amorphous phases corresponding to the third crystallization stage. The mean particle sizes of the crystallites are about 20 to 40 nm and the thickness of the intergranular amorphous phase is about 10 to 30 nm. The Nd concentration in the amorphous phase is analyzed to be about 14 at% which is much higher than the nominal Nd concentration. The increase in thermal stability of the remaining amorphous phase caused by the enrichment of Nd seems to be the reason for the maintenance of the nanostructure in the rather high temperature range of 923 to 1023 K.

(4) The bcc-Fe and $Fe_{14}Nd_2B$ phases have ferromagnetism and their Curie temperatures are measured to be about 1040 and 630 K, respectively.

(5) The nanoscale $Fe_{14}Nd_2B$ particles are surrounded by the bcc-Fe and remaining amorphous phases. It is therefore concluded that the bcc-Fe and remaining amorphous phases play an important role in the achievement of the hard magnetic properties as an effective magnetic exchange-coupled medium.

REFERENCES

(1) K. Suzuki, N. Kataoka, A. Inoue, A. Makino and T. Masumoto: Mater. Trans., JIM, **31** (1990), 743.
(2) K. Suzuki, A. Makino, N. Kataoka, A. Inoue and T. Masumoto: Mater. Trans., JIM, **32** (1991), 93.
(3) K. Suzuki, A. Makino, A. Inoue and T. Masumoto: J. Appl. Phys., **70** (1991), 6232.
(4) K. Suzuki, A. Makino, A. Inoue and T. Masumoto: Jpn. J. Appl. Phys., **30** (1991), L1729.
(5) K. Suzuki, A. Makino, A. Inoue and T. Masumoto: Mater. Trans., JIM, **32** (1991), 961.
(6) A. Makino, Y. Yamamoto, A. Inoue and T. Masumoto: Mater. Sci. Eng., **A181/A182** (1994), 495.
(7) A. Makino, A. Inoue and T. Masumoto: Nanostructured Materials, **6** (1995), 985.
(8) A. Inoue, A. Takeuchi, A. Makino and T. Masumoto: Mater. Trans., JIM, **36** (1995), 676.
(9) E. F. Kneller and R. Hawig: IEEE Trans. Magn., **27** (1991), 3588.
(10) Z. W. Li, X. Z. Zhou and A. H. Morrish: Hyperfine Interactions, **72** (1992), 111.
(11) J. Ding, P. G. McCormick and R. Street: J. Magn. Magn. Mat., **124** (1993), 1.
(12) H. Kanekiyo and S. Hirosawa: J. Magn. Soc. Jpn, **17** (1993), 185.
(13) T. Yoneyama, O. Kohmoto and K. Yajima: *Proc. of the 9th Int'l Workshop on Rare-Earth Permanent Magnets and Their Applications*, Bad Soden, FRG, (1987), p. 495.
(14) F. Matsumoto, H. Sakamoto, M. Komiya and M. Fujikura: J. Appl. Phys., **63** (1988), 3507.
(15) H. Yamamoto, M. Nagakura, Y. Ozawa and T. Katsuno: *Proc. of the 10th Int'l Workshop on Rare Earth Magnet and Their Applications*, Kyoto, Japan (1989), p. 315.
(16) H. Yamamoto and I. Kodama: Bulletin Japan Inst. Metals, **31** (1992), 52.
(17) T. Yoneyama, H. Nakamura, A. Fukuno and K. Yajima: Bulletin Japan Inst. Metals, **31** (1992), 57.
(18) N. Takahashi, S. Sugimoto, M. Okada and M. Honma: T. IEE Japan, **113-A** (1993), 251.
(19) A. Manaf, R. A. Buckley and H. A. Davies: J. Magn. Magn. Mater., **128** (1993), 302.
(20) L. Withanawasam, A. S. Murphy, G. C. Hadjipanyis and R. F. Krause: J. Appl. Phys., **78** (1994), 7065.
(21) M. Sagawa, S. Fujimura, N. Togawa, H. Hamamoto and Y. Matsuura: J. Appl. Phys., **55** (1984), 2083.
(22) Y. Matsuura, S. Hirosawa, H. Yamamoto, S. Fujimura, M. Sagawa and K. Osamura: Jpn. J. Appl. Phys., **24** (1985), L635.
(23) K. Nagayama, H. Ino and T. Umeda: J. Japan Inst. Metals, **54** (1990), 720.
(24) *Metals Databook*, ed. by Japan Inst. Metals, Maruzen, Tokyo (1983), p. 10.
(25) L. X. Liao and Z. Altounian: J. Appl. Phys., **66** (1989), 768.
(26) E. Callen, Y. J. Liu and J. R. Cullen: Phys. Rev., **B16** (1977), 263.
(27) M. C. Chi and R. Alben: J. Appl. Phys., **48** (1977), 2987.
(28) H. Fukunaga and H. Inoue: Seminar on Magnetics, IEE Japan, **MAG-90** (1990), 195.
(29) G. Herzer: IEEE Trans. Magn., **5** (1990), 1409.
(30) A. Makino, M. Yokoyama, N. Hasegawa, A. Inoue and T. Masumoto: Jpn. J. Appl. Phys., to be submitted.
(31) K. Hono, Y. Zhang, A. P. Tsai, A. Inoue and T. Sakurai: Scripta Metall. Mater., **32** (1995), 191.
(32) K. Hono. Y. Zhang, A. Inoue and T. Sakurai: Mater. Trans., JIM, **36** (1995), 909.
(33) A. Inoue: Mater. Trans., JIM, to be submitted.